Journal of The Electrochemical Society, **156** (5) H356-H360 (2009)
0013-4651/2009/156(5)/H356/5/$23.00 © The Electrochemical Society

Fabrication and Characterizations of Black Hybrid Silicon Nanomaterials as Light-Trapping Textures for Silicon Solar Cells

Chin-Lung Cheng,[a,*,z] Chien-Wei Liu,[b] Jin-Tsong Jeng,[c] Bau-Tong Dai,[b] and Yen-His Lee[a]

[a]*Institute of Mechanical and Electro-Mechanical Engineering and* [c]*Department of Computer Science and Information Engineering, National Formosa University, Huwei, Yunlin 63201, Taiwan*
[b]*National Nano Device Laboratories, Tainan 74147, Taiwan*

The effects of antireflective coatings on solar cell surfaces on photovoltaic characteristics are important issues. A comparative study of black hybrid silicon (Si) nanomaterials (BHSNMs) is demonstrated via the vapor–liquid–solid reaction using gold as the mediating catalyst and silane as the Si source ambient. By developing proper growth conditions, the study demonstrates BHSNMs with excellent antireflective characteristics. Results of this study reveal that the BHSNMs with a crisscrossed silicon rod microstructure and nanostructured texture provide excellent light trapping. Raman spectra show that the crystal structure of BHSNMs transits from single-crystalline Si to mixed amorphous Si with polycrystalline Si with increasing SiH_4 flow time. In addition, BHSNM reflections were lower than 0.4% for the 200–1100 nm wavelength range by suitably adjusting growth time. A conversion efficiency of around 1.34% with a 4.75 mA/cm^2 photocurrent V_{oc} of 400 mV and fill factor of 70.37% for the BHSNM solar cells was demonstrated. Experimental results indicate that the BHSNMs provide excellent light trapping and can be used as a promising antireflective material for solar cell applications.
 [DOI: 10.1149/1.3095479]

Manuscript submitted September 22, 2008; revised manuscript received February 9, 2009. Published March 19, 2009.

Because solar radiation is natural energy, various solar cells have become strongly competitive for terrestrial applications. An antireflective coating (ARC), the window layer, the absorber layer, the metal contact layer, and the substrate have generally been included in the solar cell. Each constituent material has different chemical and physical characteristics. A crucial understanding of the behavior of these individual components is essential for designing a device. ARCs have been widely used to increase short-circuit current density by reducing reflection at solar cell surfaces.[1-3] Moreover, researchers usually perform surface texturization to provide efficient light scattering and subsequent light absorption enhancement in the absorber material of the solar cell.[4-9] Using the subwavelength inverted pyramid gratings on single-crystalline silicon wafers obtains a 2–10% reflection.[7] Therefore, the concept of an ARC with a textured surface is a promising approach to solar cell fabrication, especially for cells with very high performance.[10] Recent studies report various forms of texturing, including reactive ion etching (RIE),[11,12] porous-Si etching,[13] wet-etching textured surfaces,[5] and photolithographically defined etching.[14] However, texturizing RIE processes cause a heavily damaged surface layer and surface chemical contamination could be caused by the wet-etching approach. Moreover, silicon-based nanowires and nanorods have become promising candidates for future scaling of advanced nanoelectronic devices due to their excellent gate control and short channel effects in metal–oxide semiconductors. Recent studies show that silicon-based nanowire propagation in solar cell applications achieved much lower reflectance through silicon nanowire arrays.[15-17] The solar cell with miniaturization is a promising candidate as an integrated power source for nanoelectronic systems.[18-20] This work achieves design optimization for light-trapping structures. Black hybrid silicon nanomaterials (BHSNMs) combined with the crisscrossed silicon rod microstructure (CSRM) with the nanostructured texture (NST) formed on the polycrystalline silicon (pc-Si)/SiO_2/Si(100) substrate demonstrated a significantly decreased reflection in the 200–1100 nm wavelength range. The BHSNMs that combined the CSRM with the NST provided excellent light trapping that can be used as a promising antireflective material for solar cell applications.

Experimental

To investigate BHSNM formation which combined the CSRM with the NST, 1.5 × 1.5 cm square samples were cut from a 6 in., (100)-oriented p-type silicon wafer with ρ = 0.1–1 Ω cm. Prior to silicon dioxide (SiO_2) growth, all wafers were cleaned with a wet cleaning process [APM (=$NH_4OH/H_2O_2/H_2O$)/HPM (=$HCl/H_2O_2/H_2O$)/DHF (=HF/H_2O)] carried out in a thermal furnace using H_2O vapor of 15 slpm at 1000°C for 120 min. The experiment thermally grew the SiO_2 layer with 500 nm thickness measured by spectroscopic ellipsometry on the cleaned wafers as a buffer layer. This study used the SiO_2/Si stack structure to demonstrate the glass substrate for thin-film solar cell applications. Then a 300 nm thick pc-Si was deposited continuously. The research was carried out at growth conditions of 620°C in 60 sccm SiH_4 ambient with a partial pressure of 200 mTorr for 120 min. The Au catalysts with (a) 5 and (b) 10 nm were deposited by a reactive dc magnetron sputtering of a Au target. Then the Au/Si(100) substrates were formed at 620°C in nitrogen ambient with a partial pressure of 100 mTorr for 20 min and were subsequently executed at 620°C in (a) mixed 100 sccm SiH_4 with 400 sccm N_2 with a partial pressure of 400 mTorr, (b) mixed 40 sccm SiH_4 with 160 sccm N_2 at a partial pressure of 400 mTorr, (c) mixed 80 sccm SiH_4 with 320 sccm N_2 at a partial pressure of 400 mTorr, (d) mixed 80 sccm SiH_4 with 320 sccm N_2 with a partial pressure of 300 mTorr, as well as (e) 300 sccm SiH_4 with a partial pressure of 350 mTorr, respectively, for 60 min. To investigate the effects of growth time on optical and physical characteristics of the BHSNMs, the experiment also deposited 10 nm Au catalysts by a reactive dc magnetron sputtering of a Au target. Next, the Au/pc-Si/SiO_2/Si(100) substrates formed at 620°C in the nitrogen ambient with a partial pressure of 100 mTorr for 20 min. Subsequently, Au/pc-Si/SiO_2/Si(100) was executed at 620°C in the 300 sccm SiH_4 with a partial pressure of 350 mTorr for 5, 15, 40, and 60 min, respectively. The pc-Si/SiO_2/Si(100) stack structure without Au catalyst was also executed at 620°C in 300 sccm SiH_4 with a partial pressure of 350 mTorr for 60 min as reference. To demonstrate the photovoltaic characterizations of the BHSNMs, both BHSNM/pc-Si/p-Si(100) and pc-Si/p-Si(100) structures were formed by phosphorus diffusion at 950°C for 4 h, respectively, resulting in an emitter with a depth of around 70 nm. The BHSNMs were executed at 620°C in 100 sccm SiH_4 at a partial pressure of 350 mTorr for 15 min. The front and rear Al contacts were formed by sputtering. Finally, sintering was conducted in a N_2/H_2 ambient at 450°C for 30 min. This study evaluated all samples using secondary electron microscopy (SEM), Raman spectrometry, X-ray diffraction (XRD), UV/visible/near IR spectrometry, and current–voltage measurement, respectively.

* Electrochemical Society Active Member.
[z] E-mail: chengcl@nfu.edu.tw

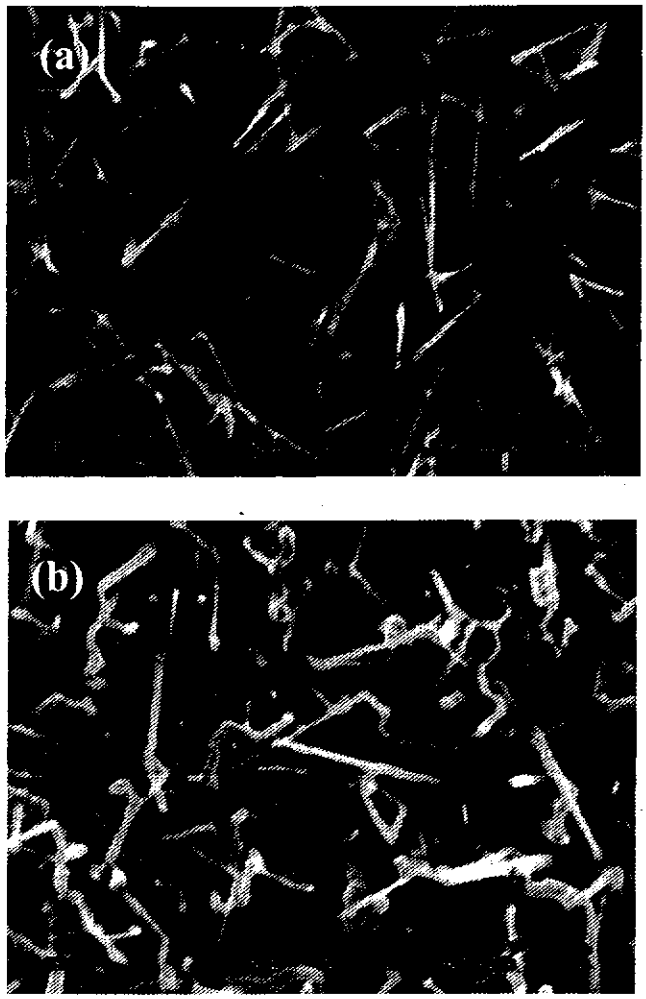

Figure 1. Plane-view SEM images of the crisscrossed silicon rods (CSRs) formed on the Au/Si(111) stack structures with a Au catalyst thickness of (a) 5 and (b) 10 nm, respectively. The growth conditions were carried out at 620°C in the mixed 100 sccm SiH_4 with 400 sccm N_2 ambient for 60 min. The SiH_4 partial pressure was achieved at 400 mTorr.

Results and Discussion

To investigate preparing BHSNMs formed with the CSRM structure, plane-view SEM images of the CSRM were formed on Au/Si(100) stack structures with Au catalyst thickness of (a) 5 and (b) 10 nm, respectively, as shown in Fig. 1. The experiment was carried out at growth conditions of 620°C in mixed 100 sccm SiH_4 with 400 sccm N_2 ambient for 60 min, achieving partial pressure in the SiH_4 at 400 mTorr. Figure 1 demonstrates that the CSRM with a diameter less than 1 μm formed on the Au/Si(100) stack structures with Au catalyst thickness of (a) 5 and (b) 10 nm, respectively. The percentage of SiH_4 in $SiH_4 + N_2$ ambient was 20% [$SiH_4/(SiH_4 + N_2) = 0.20$]. Results show that CSRM density increases with increasing Au catalyst thickness. Figure 1 results indicate that Au catalyst thickness of 10 nm was used for further investigation. Figure 2 shows the plane- and oblique-view SEM images of the CSRM formed on Au/Si(100) stack structures with Au catalyst thickness of 10 nm. The experiment was carried out at growth conditions of 620°C in (a) mixed 40 sccm SiH_4 with 160 sccm N_2, (b) mixed 80 sccm SiH_4 with 320 sccm N_2, (c) mixed 80 sccm SiH_4 with 320 sccm N_2, and (d) 300 sccm SiH_4 ambient for 60 min. The SiH_4 partial pressures were performed at (a) 400, (b) 400, (c) 300, and (d) 350 mTorr, respectively. Compared to Fig. 1b, CSRM densities decrease with decreasing SiH_4 and nitrogen flow rate under the same

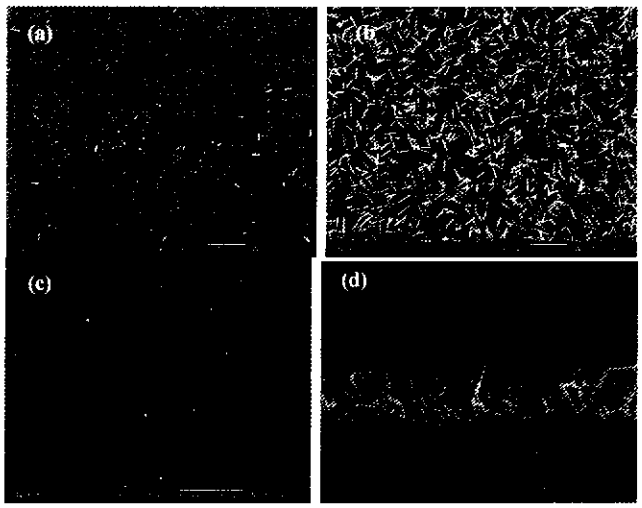

Figure 2. Plane- and oblique-view SEM images of the CSRs formed on the Au/Si(111) stack structures with Au catalyst thickness of 10 nm. The growth conditions were carried out at 620°C in (a) mixed 40 sccm SiH_4 with 160 sccm N_2, (b) mixed 80 sccm SiH_4 with 320 sccm N_2, (c) mixed 80 sccm SiH_4 with 320 sccm N_2, and (d) 300 sccm SiH_4 ambient for 60 min. The SiH_4 partial pressures were performed at (a) 400, (b) 400, (c) 300, and (d) 350 mTorr, respectively.

SiH_4 percentage (20%), as Fig. 2a and b demonstrates. Moreover, Fig. 2c shows that the CSRM cannot form with decreasing partial pressure. Therefore, achieving larger diameter and higher CSRM density requires suitably adjusting the larger SiH_4 flow rate, the thicker Au catalyst thickness, as well as the partial pressure due to a larger Si source reacting with the thicker Au catalyst. According to the above results, BHSNMs formed with the CSRM structure on the Au/Si(100) stack structure under 100% SiH_4, as Fig. 2d shows, further confirming growth time effects on optical and physical characteristics of BHSNMs investigated and shown as the following.

Figure 3a and b results illustrate the morphology of BHSNMs formed on the Au/pc-Si/SiO_2/Si(100) at 620°C in 300 sccm SiH_4 ambient with a partial pressure of 350 mTorr for (a) 5 and (b)

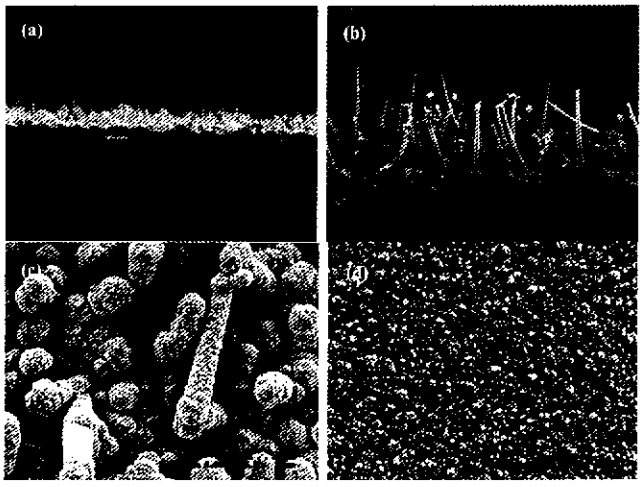

Figure 3. Oblique-view SEM images of the BHSNM formed on the Au/pc-Si/SiO_2/Si(100) stack structures with a Au catalyst thickness of 10 nm. The growth conditions were carried out at 620°C in 300 sccm SiH_4 ambient with a partial pressure of 350 mTorr for (a) 5, (b) 60, and (c) 60 min, respectively. (d) Plane-view SEM image of pc-Si/SiO_2/Si(100) stack structures without the Au catalyst carried out at 620°C in 300 sccm SiH_4 ambient with a partial pressure of 350 mTorr for 60 min.

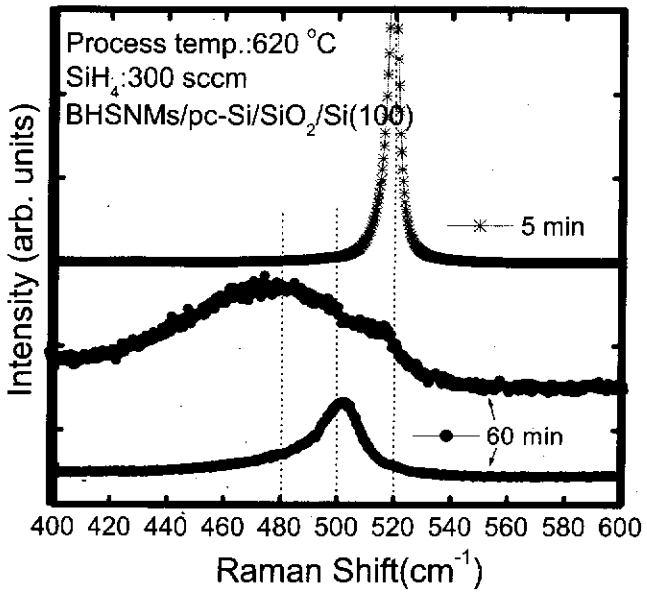

Figure 4. Raman spectra of BHSNMs formed on the Au/pc-Si/SiO_2/Si(100) stack structures with a Au catalyst thickness of 10 nm. The growth conditions were carried out at 620°C in 300 sccm SiH_4 ambient with a partial pressure of 350 mTorr for 5 and 60 min, respectively. All Raman spectral peaks of the BHSNMs for the SiH_4 flow time of 5 min are located at 520 cm^{-1}. Both the a- and pc-Si were obtained in the BHSNMs with SiH_4 flow times of 60 min on the different positions.

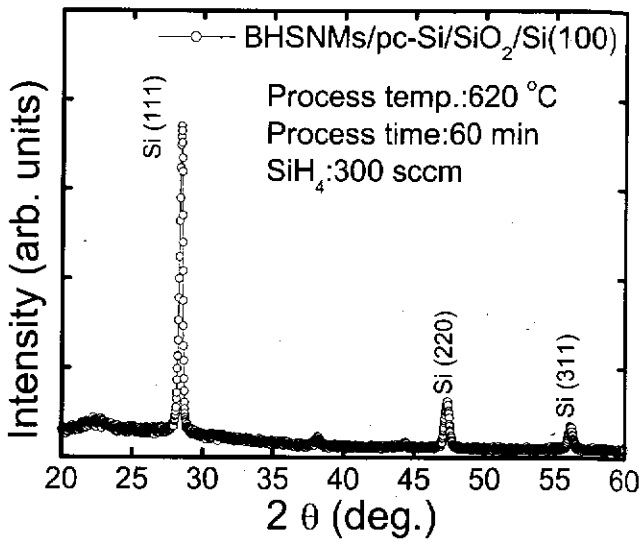

Figure 5. XRD spectra of the BHSNMs formed on the Au/pc-Si/SiO_2/Si(100) stack structures with a Au catalyst thickness of 10 nm. The growth conditions were carried out at 620°C in 300 sccm SiH_4 ambient and with a partial pressure of 350 mTorr for 60 min.

60 min, respectively. Results suggest that the density, diameter, and length increase with increasing SiH_4 flow time. Moreover, this work achieves larger diameter and higher density of the CSRM by suitably adjusting the larger SiH_4 flow rate, the thicker Au catalyst thickness, as well as the partial pressure due to a larger amount of the Si source reacting with the thicker Au catalyst. The SEM images in Fig. 3c also show that the whole and individual surface morphologies of the BHSNMs, at 620°C in the 300 sccm SiH_4 ambient with a partial pressure of 350 mTorr for 60 min, were the CSRM and the NST, respectively. Researchers report achieving larger pyramids, including side base size and pyramid height, by optimum etching processing conditions and 16% reflection for the 400–800 nm wavelength range.[21] This work obtains the CSRM with an aspect ratio of around 20:1. The CSRM with a larger aspect ratio plays a main role in light trapping, further confirming light-trapping properties in BHSNMs measured and shown in the following. A nanoscale texturing of silicon surfaces prepared by a wet chemical process also results in low reflection, leading to black Si surfaces.[22] This work obtains BHSNMs by the vapor–liquid–solid technique. To understand the BHSNM growth mechanism, Fig. 3d shows an SEM of the planar BHSNM/pc-Si/SiO_2/Si(100) stack structures without Au catalyst treated at 620°C in the 300 sccm SiH_4 ambient with a partial pressure of 350 mTorr for 60 min. A roughly textured surface was observed; however, the CSRM was not obtained. Thus, the BHSNMs combined with the CSRM and the NST can be achieved by the Au catalyst formed on the pc-Si/SiO_2/Si(100) stack structures.

Figure 4 examines the Raman spectra to demonstrate the crystalline structure of BHSNMs. Studies report that the spectra present Raman peaks centered at 520 and 504 cm^{-1} as the crystalline silicon (c-Si) and the nanocrystalline silicon (nc-Si), respectively.[23,24] The Raman peaks ranging at 500–520 and 480–500 cm^{-1} are recognized as the pc-Si and the amorphous silicon (a-Si), respectively.[25] Results show that all Raman spectral peaks of the BHSNMs for a SiH_4 flow time of 5 min (denoted by 5 min curve) in Fig. 4 are located at 520 cm^{-1}, indicating that the c-Si characteristics of the BHSNMs were demonstrated in a short time (5 min in this work). On the contrary, this study obtains both the a-Si and the pc-Si in the BHSNMs with a SiH_4 flow time of 60 min (denoted by two 60 min curves). Figure 4 presents results detected on different positions. The crystal structure of BHSNMs in Fig. 4 transits from the c-Si to the mixed a-Si with the pc-Si with increasing SiH_4 flow time.

Figure 5 shows the XRD spectra of BHSNMs formed on the Au/pc-Si/SiO_2/Si(100) substrates containing three peaks, identified as Si(111), Si(220), and Si(311). The XRD spectra also indicate that BHSNMs possess different orientation. This research adopts the Scherrer equation to estimate crystalline size embedded in the BHSNMs: $L_c = 0.9\lambda/\beta \cos\theta$, where L_c is the crystalline size, λ is the wavelength, β is the full-width at half maximum, and θ is the Bragg angle. Calculated from the Scherrer equation, the crystalline size along the Si(220) and Si(311) crystal planes embedded in the BHSNMs was achieved at around 20 nm. Crystalline size along the Si(111) crystal planes is larger than those of the Si(220) and the Si(311). According to results extracted from Fig. 4 and 5, the CSRM is a hybrid silicon nanomaterial.

To investigate the effects of random texture on reflectance characteristics, the BHSNMs formed on the Au/pc-Si/SiO_2/Si(100) substrate were performed by reflectance spectra. The reflectance spectra confirm that BHSNM reflections formed on the Au/pc-Si/SiO_2/Si substrate with various times were all lower than $<1.3\%$ for the 200–1100 nm wavelength range as shown in Fig. 6a. The BHSNM reflection formed on the Au/pc-Si/SiO_2/Si(100) substrate with 40 min is the smallest among four different treatment times in the 200–1100 nm wavelength range. Therefore, in this work a design optimization for light-trapping structures formed on the Au/pc-Si/SiO_2/Si(100) substrate was achieved in the visible region under SiH_4 flow time of around 40 min with a reflection lower than 0.4%. Figure 6b shows the reflectance spectra of the pc-Si/SiO_2/Si(100) substrates. Observations show larger reflections in the pc-Si/SiO_2/Si(100) substrate for the 200–1100 nm wavelength range. Thus, reflective characteristics were enhanced by BHSNMs formed on the Au/pc-Si/SiO_2/Si(100) due to the combined CSRM with the NST.

Figure 7 shows the reflectance spectra of BHSNMs formed on the Au/pc-Si/SiO_2/Si(100) stack structures with a Au catalyst thickness of 10 nm and without the Au catalyst, respectively. The structures of BHSNM/pc-Si/SiO_2/Si(100) and BHSNMs/Au/pc-Si/SiO_2/Si(100) were the CSRM microstructure and the planar structure, respectively, as shown in Fig. 3b and d. Compared to the

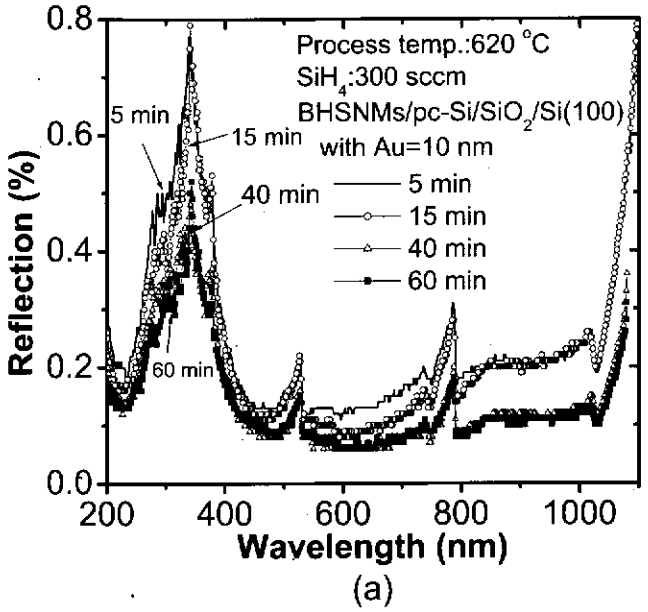

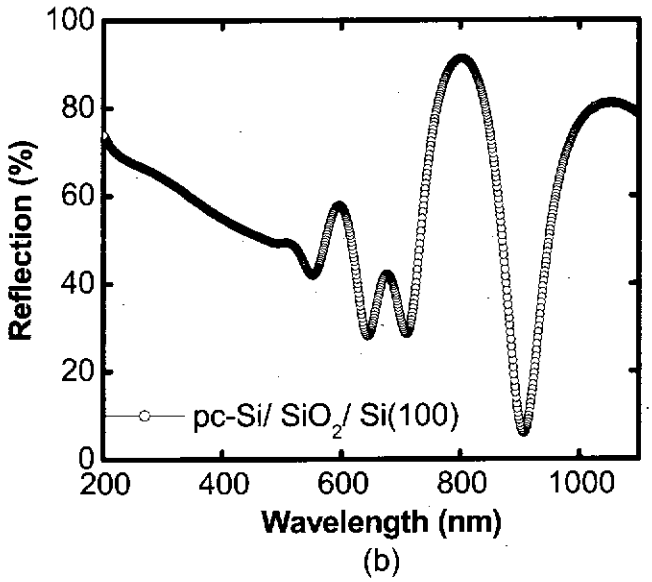

Figure 6. (a) Reflectance spectra of BHSNMs formed on the Au/pc-Si/SiO_2/Si(100) stack structures with a Au catalyst thickness of 10 nm. The growth conditions were carried out at 620°C in 300 sccm SiH_4 ambient with a partial pressure of 350 mTorr for 5, 15, 40, and 60 min, respectively. (b) The reflectance spectra of the pc-Si/SiO_2/Si(100) stack structures as reference is shown.

planar BHSNM/pc-Si/SiO_2/Si(100), the reflection of the BHSNM/Au/pc-Si/SiO_2/Si(100) sample with a Au catalyst thickness of 10 nm sample is much smaller due to BHSNMs with the CSRM structure. The reflections in the near-infrared region were particularly reduced by the CSRM of BHSNMs.

Figure 8 shows dark and illuminated (AM 1.5) current density–voltage curves for the devices with (a) n^+-BHSNMs/i-BHSNMs/pc-Si/p-Si(100) and (b) n^+-pc-Si/pc-Si/p-Si(100) structures, respectively. The Air Mass is defined as AM = $1/\cos\theta$, where θ is the angle from the vertical (zenith angle). The efficiencies were measured under the global AM 1.5 spectrum (1000 W/m^2) at 25°C. A conversion efficiency of around 1.34% with a 4.75 mA/cm^2 photocurrent V_{oc} of 400 mV and fill factor (FF) of 70.37% for the BHSNM solar cell was obtained as shown in Fig. 8. Compared to the

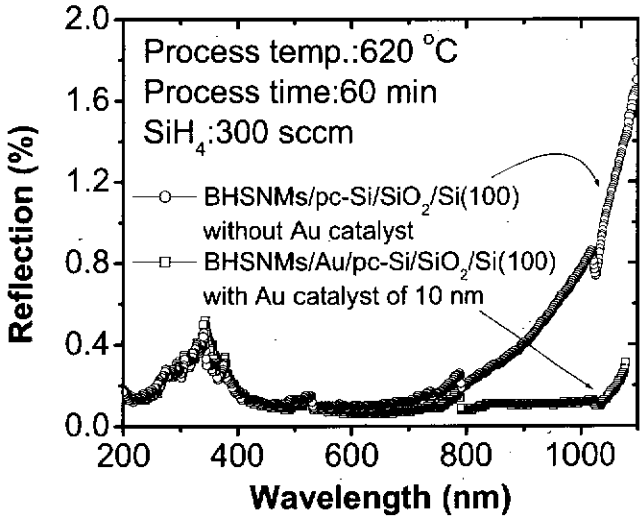

Figure 7. Reflectance spectra of BHSNMs/pc-Si/SiO_2/Si(100) without Au catalyst and BHSNMs/Au/pc-Si/SiO_2/Si(100) stack structures with a Au catalyst thickness of 10 nm, respectively. The growth conditions were carried out at 620°C in 300 sccm SiH_4 ambient with a partial pressure of 350 mTorr for 60 min.

planar n^+-pc-Si/pc-Si/p-Si(100) structured solar cell, the BHSNM solar cell had conversion efficiency improvement of ~34%.

Conclusions

BHSNMs were grown via the vapor–liquid–solid reaction using gold (Au) as the mediating catalyst and silane (SiH_4) as the Si source ambient. An SEM image displays the entire structure and individual surface morphologies of the BHSNMs as CSRM and NST, respectively. Raman spectra show that the crystal structure of the BHSNMs transits from a single c-Si to mixed a-Si with the pc-Si with increasing SiH_4 flow time. The XRD spectra indicate the BHSNMs formed on the Au/pc-Si/SiO_2/Si(100) contain three peaks, identified as Si(111), Si(220), and Si(311) crystal planes. The reflectance spectra confirm that BHSNM reflections deposited on the Au/pc-Si/SiO_2/Si(100) substrate by suitably adjusting growth time were all lower than 0.4% for the 200–1100 nm wavelength range

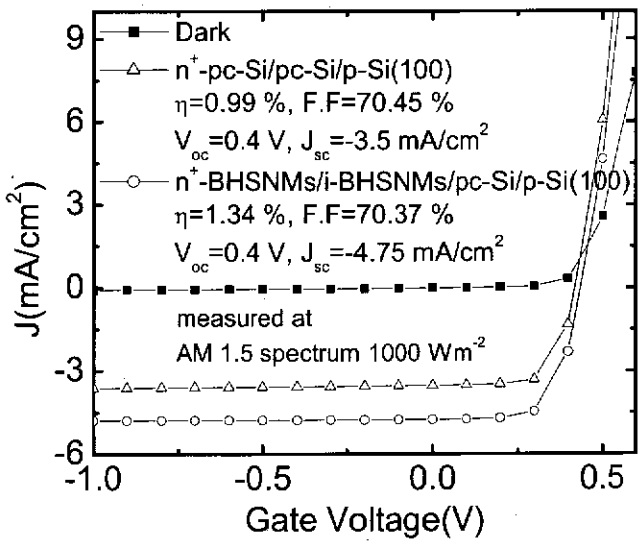

Figure 8. Dark and illuminated (AM 1.5) current density–voltage curves for the devices with the n^+-BHSNMs/i-BHSNMs/pc-Si/p-Si(100) and the n^+-pc-Si/pc-Si/p-Si(100) structures, respectively.

due to combined CSRM with NST. A conversion efficiency of around 1.34% with a 4.75 mA/cm^2 photocurrent V_{oc} of 400 mV and FF of 70.37% for the BHSNM solar cell was demonstrated. Experimental results indicate that the BHSNMs provide excellent light trapping and can be used as a promising antireflective material for solar cell applications.

Acknowledgments

The authors thank the National Science Council of the Republic of China for the financial support under contract no. NSC 95-2221-E-150-092, NSC 96-2221-E-492-012-MY3, no. NSC 97-2221-E-150-072, and no. NSC 96-2221-E-150-070-MY3. Technical support from National Nano Device Laboratories (NDL) of China is also acknowledged.

National Formosa University assisted in meeting the publication costs of this article.

References

1. T. T. Minemoto, T. Mizuta, H. Takakura, and Y. Hamakawa, *Sol. Energy Mater. Sol. Cells*, **91**, 191 (2007).
2. Z. Chen, P. Sana, J. Salami, and A. Rohatgi, *IEEE Trans. Electron Devices*, **40**, 1161 (1993).
3. J. Zhao, A. Wang, and M. A. Green, *IEEE Trans. Electron Devices*, **41**, 1592 (1994).
4. J. Zhao, A. Wang, P. Campbell, and M. A. Green, *IEEE Trans. Electron Devices*, **46**, 1495 (1999).
5. U. Gangopadhyay, K. H. Kim, S. K. Dhungel, U. Manna, P. K. Basu, M. Banerjee, H. Saha, and J. Yi, *Sol. Energy Mater. Sol. Cells*, **90**, 3557 (2006).
6. Y. Ein-Eli, N. Gordon, and D. Starosvetsky, *Sol. Energy Mater. Sol. Cells*, **90**, 1764 (2006).
7. C. H. Sun, W. L. Min, N. C. Linn, P. Jiang, and B. Jiang, *Appl. Phys. Lett.*, **91**, 231105 (2007).
8. C. Rockstuhl, F. Lederer, K. Bittkau, and R. Carius, *Appl. Phys. Lett.*, **91**, 171104 (2007).
9. C. Haase and H. Stiebig, *Appl. Phys. Lett.*, **91**, 061116 (2007).
10. K. Tsujino and M. Matsumura, *Sol. Energy Mater. Sol. Cells*, **90**, 1527 (2006).
11. W. A. Nositschka, O. Voigt, P. Manshanden, and H. Kurz, *Sol. Energy Mater. Sol. Cells*, **80**, 227 (2003).
12. H. L. Chen, K. T. Huang, C. H. Lin, W. Y. Wang, and W. Fan, *Microelectron. Eng.*, **84**, 750 (2007).
13. R. R. Bilyalov, L. Stalmans, L. Schirone, and C. Levy-Clement, *IEEE Trans. Electron Devices*, **46**, 2035 (1999).
14. J. Zhao, A. Wang, M. A. Green, and F. Ferrazza, *Appl. Phys. Lett.*, **73**, 1991 (1998).
15. L. Hu and G. Chen, *Nano Lett.*, **7**, 3249 (2007).
16. B. M. Kayes, M. A. Filler, M. C. Putnam, M. D. Kelzenberg, N. S. Lewis, and H. A. Atwater, *Appl. Phys. Lett.*, **91**, 103110 (2007).
17. C. L. Cheng, C. W. Liu, Y. H. Lee, J. T. Jeng, and B. T. Dai, in *The 4th Asian Conference on Crystal Growth and Crystal Technology (CGCT4)*, Japan, Abstract ID 208 (2008).
18. L. Tsakalakos, J. Balch, J. Fronheiser, B. A. Korevaar, O. Sulima, and J. Rand, *Appl. Phys. Lett.*, **91**, 233117 (2007).
19. B. Tian, X. Zheng, T. J. Kempa, Y. Fang, N. Yu, G. Yu, J. Huang, and C. M. Lieber, *Nature (London)*, **449**, 885 (2007).
20. T. Stelzner, M. Pietsch, G. Andra, F. Falk, E. Ose, and S. Christiansen, *Nanotechnology*, **19**, 295203 (2008).
21. E. Fornies, C. Zaldo, and J. M. Albella, *Sol. Energy Mater. Sol. Cells*, **87**, 583 (2005).
22. S. Koynov, M. S. Brandt, and M. Stutzmann, *Appl. Phys. Lett.*, **88**, 203107 (2006).
23. B. Li, D. Yu, and S. L. Zhang, *Phys. Rev. B*, **59**, 1645 (1999).
24. M. Lu, M. K. Li, L. B. Kong, X. Y. Guo, and H. L. Li, *Composites, Part B*, **35**, 179 (2004).
25. T. C. Wong, C. H. Yu, and J. J. Wu, *J. Cryst. Growth*, **243**, 419 (2002).